

Stage-specific tumor microenvironment dynamics and cancer-associated fibroblast profiling in MBL-6 mouse models of breast cancer

Ladan Langroudi, Maryam Iranpour, Mojtaba Mollaei, Masoud Soleimani, Seyed Mahmoud Hashemi, Zuhair M. Hasan Masoud Soleimani, Maryam Iranpour, Mojtaba Mollaei, Masoud Soleimani, Masoud Soleimani, Masoud Hashemi, Masoud Hashemi, Masoud Soleimani, Masoud Hashemi, Masoud H

¹Department of Immunology, School of Medicine, Kerman University of Medical Sciences, Kerman, Iran; ²Department of Pathology, School of Medicine, Kerman University of Medical Sciences, Kerman, Iran; ³Department of Microbiology and Immunology, University of Montreal, Canada; ⁴Department of Hematology, Faculty of Medical Sciences, Tarbiat Modares University, Tehran, Iran; ⁵Department of Immunology, School of Medicine, Shahid Beheshti University of Medical Sciences, Tehran, Iran; ⁶Department of Immunology, Faculty of Medical Sciences, Tarbiat Modares University, Tehran, Iran

Abstract

Breast cancer remains the most prevalent malignancy among women, necessitating the development of novel therapeutic strategies. Experimental animal models that closely mimic human

Correspondence: Professor Zuhair M. Hasan, Department of Immunology, Faculty of Medical Sciences, Tarbiat Modares University, Jalal Highway, Tehran, Iran. E-mail: hasan_zm@modares.ac.ir

Key words: MBL-6; TNM staging; carcinoma-associated fibroblasts; COX-2; mouse model.

Contributions: LL, conceptualization, formal analysis, methodology, investigation, writing – original draft, visualization, software; MI, pathologic evaluations; MM, writing; ZMH, conceptualization, formal analysis, methodology, resources, validation, supervision, writing – review & editing, funding acquisition; MS, resources, funding acquisition; SMH, formal analysis, methodology, supervision, writing – review & editing. All authors have read and approved the final version of the manuscript and agreed to be accountable for all aspects of the work.

Conflict of interest: the authors have no conflict of interest to declare.

Ethics approval: this study was approved by the ethical committee of Tarbiat Modares University.

Availability of data and materials: the datasets used and/or analyzed during the current study are available from the corresponding author on reasonable request.

Funding: this study was funded by the Research Deputy of Tarbiat Modares University.

Received: 17 June 2024. Accepted: 1 August 2025.

This work is licensed under a Creative Commons Attribution-NonCommercial 4.0 International License (CC BY-NC 4.0).

©Copyright: the Author(s), 2025 Licensee PAGEPress, Italy Veterinary Science Development 2025; 9:10069 doi:10.4081/vsd.2025.10069

Publisher's note: all claims expressed in this article are solely those of the authors and do not necessarily represent those of their affiliated organizations, or those of the publisher, the editors and the reviewers. Any product that may be evaluated in this article or claim that may be made by its manufacturer is not guaranteed or endorsed by the publisher. breast cancer are crucial for advancing these therapies. This study utilized the criteria of the tumour, node, metastasis (TNM) staging system and variations in metabolic rates to develop models representing stages II and IV of human breast cancer, using the MBL-6 mouse breast cancer cell line. We assessed tumor growth curves in vivo and investigated distant metastasis to organs such as the liver, lungs, lymph nodes, and spleen. Carcinoma-associated fibroblasts (CAFs) were isolated, and their proliferation rates, inflammatory enzyme expression, and matrix metalloproteinase levels were compared between stages II and IV. By analyzing tumor kinetics and metabolic differences, we were able to predict tumor size and progression at each stage. Our results revealed that CAFs isolated from both stages exhibited similar phenotypic characteristics. However, CAFs from stage II tumors showed higher expression of indoleamine 2,3-dioxygenase 1 (IDO1), while those from stage IV tumors had higher levels of inducible nitric oxide synthase (iNOS). These distinct expression patterns suggest unique microenvironmental features at different stages of tumor progression. Further investigation of the cancer microenvironment may provide valuable insights for selecting targeted therapies and improving disease management.

Introduction

Breast cancer is the most prevalent malignancy among women worldwide, contributing significantly to both morbidity and mortality. In 2020, an estimated 2.3 million women were diagnosed with breast cancer, and 685,000 died from the disease. Given its global impact, ongoing research into breast cancer biology, diagnosis, and treatment is crucial. Understanding the dynamic changes in cancer cell biology, their functionality, and interactions with stromal cells throughout disease progression is essential for advancing therapeutic strategies. Additionally, the development of research tools, such as cell lines and animal models, plays a vital role in improving our understanding of the disease and fostering innovation in treatment options.

To study various aspects of cancer biology and treatment before advancing to human clinical trials, both *in vitro* and *in vivo* models are essential. Cell lines and animal models are indispensable tools in this process. Among the available animal models for breast cancer, rodents, particularly mice, are the most commonly used in laboratory research.² Mice share key anatomical, physiological, and genetic similarities with humans,^{3,4} making them ideal for modeling human diseases. The availability of inbred strains and advanced gene-editing technologies further enhances the utility of mice in breast cancer research. However, it is important to account for the differences in metabolic rates between humans and mice,





which highlights the need for supplementary human studies to draw accurate conclusions. ^{5,6} Mice offer the advantage of naturally occurring spontaneous tumors ⁷ and exhibit a similar etiology to human breast cancer. ⁸ This makes mice a valuable source for widely used breast cancer cell lines. Notable examples of mouse-derived breast cancer cell lines include 4T1, EMT6, TM40, and D2A1 (derived from BALB/c mice); E0771 (from C57BL/6 mice); and MVT1, 6DT1, and M6 (from FVB mice). ⁹

One of the main challenges in using animal cancer models is the variability in the stages at which studies are conducted, leading to discrepancies between different studies. This inconsistency is often influenced by the chosen methodology and cell line. ¹⁰ The development of immunocompromised mice, such as nude mice, which lack both an immune system and hair follicles, has greatly advanced our understanding of cancer cell biology by enabling the study of human-derived cell lines *in vivo*. While these models are invaluable for pharmacological studies of new anticancer therapies, their lack of an immune system limits their utility in immunological research and immunotherapy studies. ^{11,12} Additionally, cancer cell-stroma interactions vary across different stages of human cancer, ¹³ highlighting the importance of stage-specific modeling in animal research. However, few studies have focused on modeling the distinct stages of cancer in animal models to date.

The MBL-6 cell line, isolated by our group from a spontaneous mammary tumor in BALB/c mice, offers a valuable model for breast cancer research. This model has the advantage of a long *in vivo* duration and is currently being tested for its response to anticancer drugs. Furthermore, it is well-suited for studying cancer cell-stroma interactions and cancer evolution, particularly in the context of multi-organ distant metastasis.¹⁴ In this study, we employed the tumor, node, metastasis (TNM) staging system and metabolic rate variations to establish models for stages II and IV of human breast cancer using the MBL-6 cell line. Additionally, carcinoma-associated fibroblasts (CAFs) were isolated from each stage, and their proliferative capacities and inflammatory enzyme profiles – including cyclooxygenase 2 (COX-2), indolamine deoxygenase 1 (IDO1), inducible nitric oxide synthase (iNOS), and matrix metalloproteinase 2 (MMP2) and 9 – were compared.

Materials and Methods

Establishing a model for stages II and IV

In studies involving mouse models, terms such as "early" and "late" are used to denote various stages of cancer. However, this terminology is not applicable when translating animal models into human studies. Here, we utilized the model of human tumor growth kinetics¹⁵ and considered metabolic rate differences⁵ to establish a model for stages II and IV of *in vivo* tumor growth in BALB/c mice.

According to the American Joint Commission on Cancer tumor, node, metastasis (AJCC-TNM) staging of breast cancer, ¹⁶ a combination of tumor size, lymph node involvement, and metastasis is used to classify a breast cancer stage. Specifically, the AJCC-TNM staging of human breast cancer defines stage II as a tumor size of 2-5 cm without lymph node involvement and stage IV as a tumor size greater than 5 cm with distant metastasis. In order to translate these sizes with tumor growth kinetics, tumor size was transformed to the number of cancer cells using the following equation: ¹

$$N = \frac{V_T}{V_C} = \left\{ \frac{1}{6} \pi (2W * H) \right\} / \left\{ \frac{4}{3} \pi (d/2)^3 \right\}$$

where V_T and V_C are the tumor volume (as an oblate ellipsoid) and cancer cell volume (ellipsoid shape), respectively,^{17,18} W is tumor width, H is tumor height, and d is the cancer cell diameter, which was assumed to be 10 μ m. Therefore, a human stage II breast cancer with a diameter of 2 cm has a volume of 4186.67 mm³ and 8′10° cells and a weight of 1 g. Considering the metabolic rate differences between humans and mice (estimated at a 7:1 ratio), the equivalent stage II tumor in a mouse would contain approximately 1×10^9 cancer cells. In the case of human stage IV cancer, where the primary tumor is typically absent, we adopted the ethically approved tumor burden limit of 10-15% of the animal's body weight. Based on this guideline, a stage IV tumor in a mouse would correspond to approximately 2×10^9 cells, with a mass exceeding 2 g and evidence of distant metastases.

The cell line of choice was MBL-6, which was isolated from spontaneous breast cancer of a BALB/c mouse. MBL-6 tumors possess a similar pathology to human invasive ductal carcinoma. 14 Twenty female 4-6-week-old BALB/c mice (Pasture Institute, Tehran, Iran) were subcutaneously inoculated with 5'105 MBL-6 cells. As explained above, mice were euthanized using a CO₂ chamber when the tumors reached an approximate cell number of 10° cells (stage II) and 2′10° cells (stage IV) (n=10 in each group), estimated from tumor size using a digital caliper (Mitutoyo, Japan) and the corresponding equation.1 Number of mice in each group was decided based on previous studies.¹⁹ Any animal showing signs of distress, difficulty obtaining food, or harassment by other animals was isolated or euthanized using standard protocols to minimize animal pain. Different tissues, including tumor, liver, spleen, lung, and lymph nodes, were aseptically resected and fixed in 10% formalin, and the tissues were sectioned and stained with H&E for metastasis analysis by a pathology specialist. A tumor volume of 2,000 mm³ (2 g or 10-15% body weight) was selected as the ethical endpoint of the study. Additionally, tumors were cultured for the isolation of CAFs.

Isolation of CAFs

Tumor tissues were aseptically removed, washed in phosphate-buffered saline (PBS), and minced into 1-3 mm-sized fragments. Fragments were washed in PBS and incubated in an enzyme cocktail consisting of 0.5% collagenase IV, 0.02% hyaluronidase, 0.25% trypsin, and 0.002% DNase I in DMEM/F12. After 4 hours in a shaking 37°C incubator, cell suspensions were fractioned using the Ficoll separation technique. The interface layer consisted of fibroblasts, and the pellet consisted mainly of cancer cells. Fibroblasts were separated, washed in PBS, and plated in DMEM/F12 (Gibco, Thermo Fisher Scientific, Waltham, MA, USA) supplemented with 30% fetal bovine serum (FBS; Gibco, Thermo Fisher Scientific, Waltham, MA, USA) and 1% penicillin/streptomycin (Biosera, Heathfield, UK). Fibroblastic colonies were passaged in 10% FBS DMEM/F12. Passages 2 and 3 cells were used for future evaluations.

CAFs' characterization

Immunocytochemistry (ICC) for the marker fibroblast activation protein (FAP) was used to characterize the isolated CAFs. Briefly, 10,000 CAFs were seeded in 4-well tissue culture plates. After 24 hours, CAFs were fixed with 4% paraformaldehyde (PFA) and washed with 0.1% PBS-Tween 20. Unspecific binding was blocked with 5% goat serum, and cells were immunostained





with rabbit anti-mouse FAP antibody (eBioscience, Vienna, Austria) overnight at 4°C. Fluorescein isothiocyanate (FITC)-conjugated goat anti-rabbit IgG secondary antibody was used, and cells were counterstained with nuclear stain 4',6-diamidino-2phenylindole (DAPI). Additionally, tumor tissues were immunostained for FAP expression. Paraffin-embedded tissues were sectioned and immunostained with rabbit anti-mouse FAP antibody (Abcam Ltd, Cambridge, UK). Sections were deparaffinized with heat and subsequent solutions of xylene and were hydrated using descending concentrations of alcohol (100%-50%). Antigen retrieval was performed using a sodium citrate buffer-Heat-Induced Epitope Retrieval (HIER) protocol. A 3% H₂O₂ solution and 5% goat serum were used to block endogenous peroxidase activity and non-specific binding, respectively. Primary antibody, including rabbit anti-FAP (Abcam), was added overnight at 4 °C. Horseradish peroxidase (HRP)-conjugated goat anti-rabbit IgG (Abcam) was used as a secondary antibody. Diaminobenzidine (DAB) chromogen solution was added for 20 min, and slides were counterstained with H&E. Slides were dehydrated, mounted, and evaluated for FAP staining by a pathology specialist. The properties of antibodies used in ICC and immunohistochemistry (IHC) are listed in Table 1.

Colony-forming unit and growth curve analysis

A colony-forming unit (CFU) assay was performed as follows. CAFs were resuspended in three concentrations of 100, 500, and 1,000 viable cells and in 10 mL DMEM/F12 medium and cultured in a 9 cm dish. Media was replaced biweekly. On day 14, cultures were fixed with 4% PFA and stained with crystal violet. Fibroblastic colonies with more than 50 cells and/or possessing a diameter greater than 2 mm were counted under an inverted microscope. Three isolated CAFs were evaluated in triplicate.

For growth curve analysis, CAFs were cultured at an initial density of 5,000 cells/well in 24-well plates. At 24-hour intervals, an MTT assay was performed, and the optical density was recorded. The growth curve of three isolates was evaluated for 14 consecutive days in triplicate. The optical density was quantified using a cell-standard curve.

Gene expression analysis using real-time polymerase chain reaction

Gene expression was assessed using real-time polymerase chain reaction (PCR). Total cellular RNA was extracted using Trizol (Gibco, Thermo Fisher Scientific, Waltham, MA, USA). Random hexamer-primed reverse transcription (Metabion, Germany) was performed on aliquots containing 1 µg of total RNA as a template. The resulting cDNA was used for real-time PCR amplification. Primers for COX-2, iNOS, IDO1, MMP2, and MMP9, and beta-actin were synthesized based on the reported sequences and are as follows:

COX-2 (145 bp) forward: 5'-AGACAGATCATAAGCGAGGAC-3', reverse: 5'-CCACCAATGACCTGATATTTC-3';

INOS (142 bp) forward: 5'-TGTGCGAAGTGTCAGTGG-3', reverse: 5'-TCCTTTGAGCCCTTTGTG-3';

IDO1 (168 bp) forward: 5'-GGATGCGTGACTTTGTGG-3', reverse: 5'-TGGAAGATGCTGCTCTGG-3';

MMP2 (150 bp) forward: 5'-AGACAAGTTCTGGAGATA-CAATG-3', reverse: 5'-GCACCCTTGAAGAAGTAGC; -3' MMP9 (136 bp) forward: 5'-GGCGTGTCTGGAGATTCG-3', reverse: 5'-TGGCAGAAATAGGCTTTGTC-3'.

Real-time PCR reaction mixtures (final volume: $30~\mu L$) contained $1~\mu L$ of cDNA template, $3~\mu L$ of 200 μM dNTPs, 30 pmol of each primer, and 1 unit of Taq-DNA polymerase (MBI Fermentas Inc., Burlington, ON, Canada). PCR amplification was performed under the following thermal cycling conditions: 40 cycles at 94°C for 30 s; at 55°C for 60 s; and at 72°C for 1 min, followed by a final extension step at 72°C for 10 min.

Amplification and fluorescence data were acquired using the Rotor-Gene 6000® system (Corbett Life Science, Australia), with analysis performed using Rotor-Gene Series Software v1.7 (build 34). Relative gene expression was calculated using REST software (version 2009).

Statistical analysis

The data is presented as mean ± standard error of the mean (SEM), otherwise stated. Statistical analysis was performed using SPSS v.19 software and GraphPad Prism v. 8, employing analysis of variance (ANOVA) or the Mann-Whitney test where applicable. The relative expressions and heatmap demonstration were analyzed using REST software version 2009 and R Studio, respectively. A p-value below 0.05 was regarded as statistically significant.

Results

Establishment of stage II and IV models

MBL-6 is a cell line isolated from a spontaneous invasive ductal carcinoma of the mammary glands of a BALB/c mouse. This cell line has the advantage of exhibiting long-term *in situ* growth before metastasis, allowing for various evaluations. After tumors became palpable, they were measured daily. Subcutaneous growth was measured using a digital vernier caliper (Mitutoyo, Japan), and tumor volume was converted to cell number according to the equation. When the number of estimated cells reached 1×10^9 or 2×10^9 cells, tumors were grouped as stage II and IV, respectively. The tumor growth was monitored for 45 days from inoculation until the tumor volume reached 2,000 mm³, which was the recommended ethical endpoint (Figure 1a). The TNM staging criteria are one of the most frequently used in clinics for staging and treatment of breast cancer. In this study, the tumor size, being the most

Table 1. Antibodies used in ICC and IHC staining of CAFs and tumor tissue.

Analysis	Antibody	Host	Source	Clone	Antigen retrieval	Dilution	Tag
Primary Antibody	FAP	Mouse	Abcam ab207178		Tween 20	1:100	None
Secondary antibody (ICC)	Anti-rabbit	Goat	Razi Biotech AF8035	Polyclonal	Tween 20	1:100	FITC
Secondary antibody (IHC)	Anti-rabbit	Goat	Abcam ab6721	Polyclonal	Acidic HIER	1:1000	HRP

FAP, fibroblast activation protein; ICC, immunocytochemistry; FITC, fluorescein isothiocyanate; IHC, immunohistochemistry; HIER, Heat-Induced Epitope Retrieval protocol; HRP, horse-radish peroxidase.





important criterion in TNM staging, was converted to cell number. Since a tumor size of 2 mm in humans is considered stage II, and this size is equivalent to the endpoint size in mice, the conversion of tumor size to cell number serves as a standardization of tumor size for use in the mouse model. Other criteria, such as lymph node involvement, were also assessed using macroscopic evaluations and validations by histology. Although the orthotopic model is preferable, its limited space leads to rapid metastasis development. In this regard, the subcutaneous model has a longer *in situ* growth, allowing the expansion and development of the tumor microenvironment (TME). It is noteworthy that the cell line of choice has a significant impact on the behavior of the tumor, with some exhibiting a strong metastatic ability, while others are more dormant. On the other hand, studies suggest that either orthotopic or subcutaneous models show similar CAF phenotypes.

As seen in Figure 1a, after 29-31 days, tumors reached 10^9 cells and were grouped as stage II. After 40 days, they reached 2×10^9 cells and were grouped as stage IV. At each stage, metastasis was evaluated using H&E staining and revealed increased growth of cancer cells in distant tissues in stage IV mice. As shown in Figure 1b, in stage II, metastasis to lymph nodes (4 of 10) and liver (1 of 10) showed traces of tumor cell growth, whereas in stage IV (Figure 1c), all the tissues showed traces of cancer cell growth.

Isolation of CAFs and immunostaining

Staining of CAFs in culture showed FAP expression in both stage II and IV CAFs (Figure 2 a-c). These results confirm that the isolation technique was able to efficiently isolate carcinoma-associated fibroblasts from two different stages. The IHC staining of

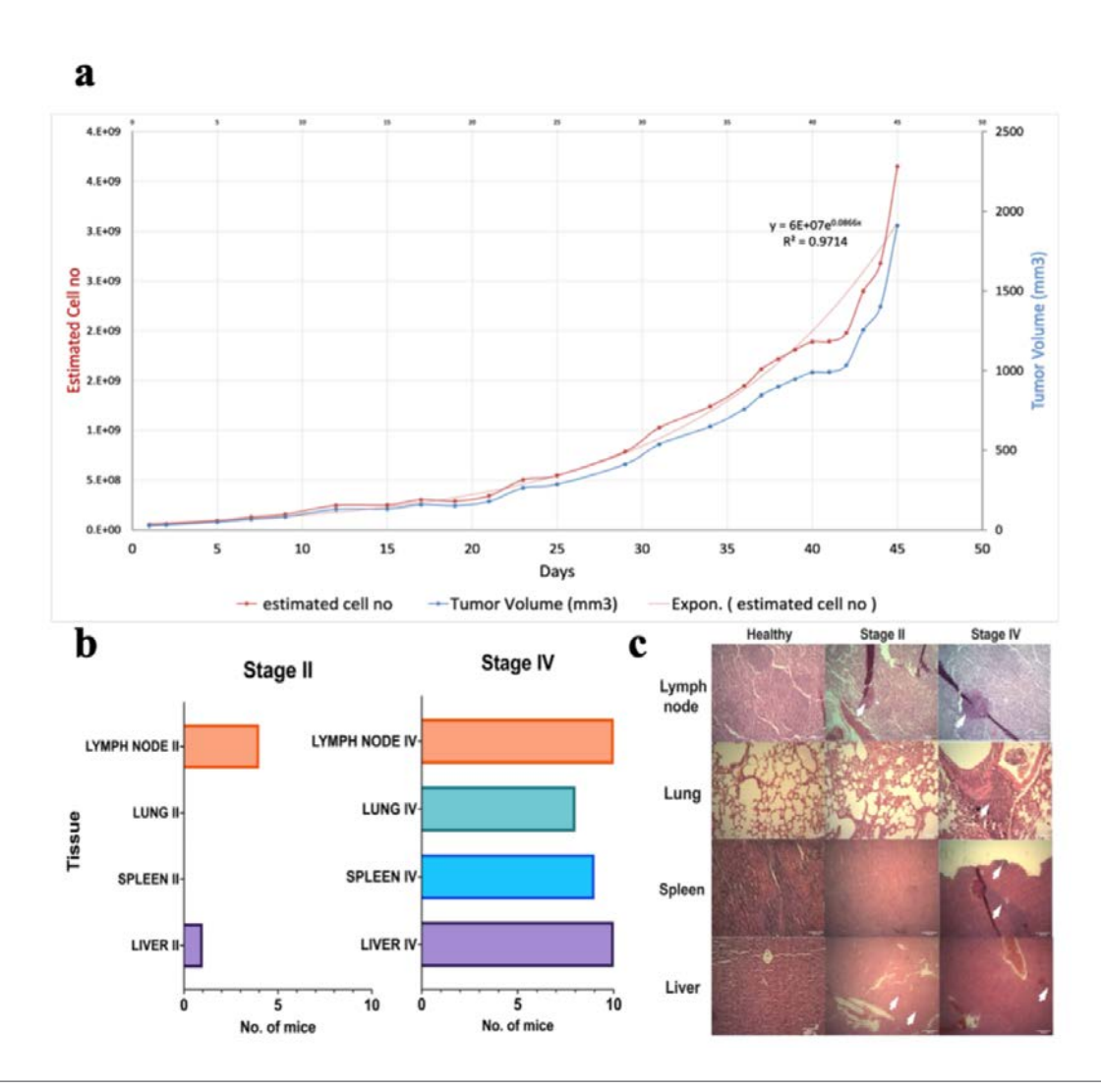


Figure 1. Stage establishment and evaluations. a) *In vivo* tumor growth curve of MBL-6 in BALB/c mice showed 100% engraftment. Tumors were measured daily using a digital vernier caliper. After 30 days, tumors reached 1×10^9 cells. These mice were grouped as stage II based on the tumor size equivalent to the TNM staging. On day 40 post inoculation, they reached 2×10^9 cells, which were grouped as stage IV. b) Macroscopic evaluations of collected tissues revealed that 4 out of 10 and 1 out of 10 mice showed metastatic growth in lymph nodes and liver, respectively. In contrast, the number of metastasis-positive tissues was higher in stage IV animals. c) Metastasis growth (arrowhead) in the liver, spleen, lung, and lymph node of stages II and IV of tumor-bearing mice was compared to healthy tissues. The H&E staining of tissue sections revealed that mice in stage II had minor metastasis to the lymph node and liver (4 of 10), while mice in stage IV showed signs of metastasis in all the tissues evaluated (n=10; scale bar = 100 μ m).



tumor tissues also showed FAP-positive cells in the tumor tissue (Figure 2 d-f), demonstrating the presence of CAFs in tissues.

Proliferative capacities of CAFs

Evaluation of CAF growth characteristics

The growth curve of isolated CAFs was assessed over a period of 14 consecutive days. Each day, the proliferation of 5000 seeded cells was determined using the MTT assay, with an MTT-cell standard curve. As depicted in Figure 3a, the growth curve of CAFs remained similar until day 8, after which CAF-IV exhibited decreased proliferation. Statistical analysis revealed that from day 11 onwards, the growth of CAF-II was significantly higher compared to CAF-IV. Calculations based on curve equations determined the doubling time of CAF-II and CAF-IV as 2.891 and 1.607 days, respectively.

Assessment of colony-forming ability

The ability of CAFs to form fibroblastic colonies was evaluated using a CFU-fibroblastic (CFU-F) assay. Figure 3b illustrates the number of CFU-F cells obtained at passage 3. The CFU-F assay was conducted using three concentrations (1,000, 500, and 100 cells), with colony counts performed in triplicate of three separate isolated CAFs. Statistical analysis revealed a significantly higher number of colonies in CAF-II cultures (p<0.001).

Inflammatory gene expression analysis

The expression of inflammatory enzymes in CAFs was com-

pared between the two stages. Gene expression analysis indicated that the level of IDO1 mRNA was significantly higher in stage II CAFs, with a mean factor of 182.9 (p=0.002). Conversely, iNOS expression was found to be significantly higher in stage IV CAFs, with a mean factor of 0.490 (p<0.01). Analysis of MMP2 and MMP9 expression revealed no significant differences between the two CAFs (p<0.05). The relative mRNA expression levels, volcano plots, and heatmap comparison are depicted in Figure 4.

Discussion

Activated stroma is observed in many cancers, and CAFs are the main component.20 The study of CAFs has increased due to their vital role in tumor progression and immune evasion of cancer. Many studies utilize patient-derived CAFs, which are cumbersome and expensive, and drug-native samples are scarce. The current animal models and cell lines also fail to provide the necessary stroma for adequate extraction and evaluation. Using tumor kinetics and metabolic rate differences, we were able to correctly predict each stage in the MBL-6 tumor-bearing mice. This enables closer observation of tumor progression and comparison of different aspects of tumor biology and treatment across various stages in animal models. In addition, the relatively moderate in vivo growth rate of this line can provide increased accuracy in experimental settings. Additionally, an attainable stroma is provided by this model, which permits TME studies. Therefore, the MBL-6 model has shown advantages for in vivo studies of the TME.

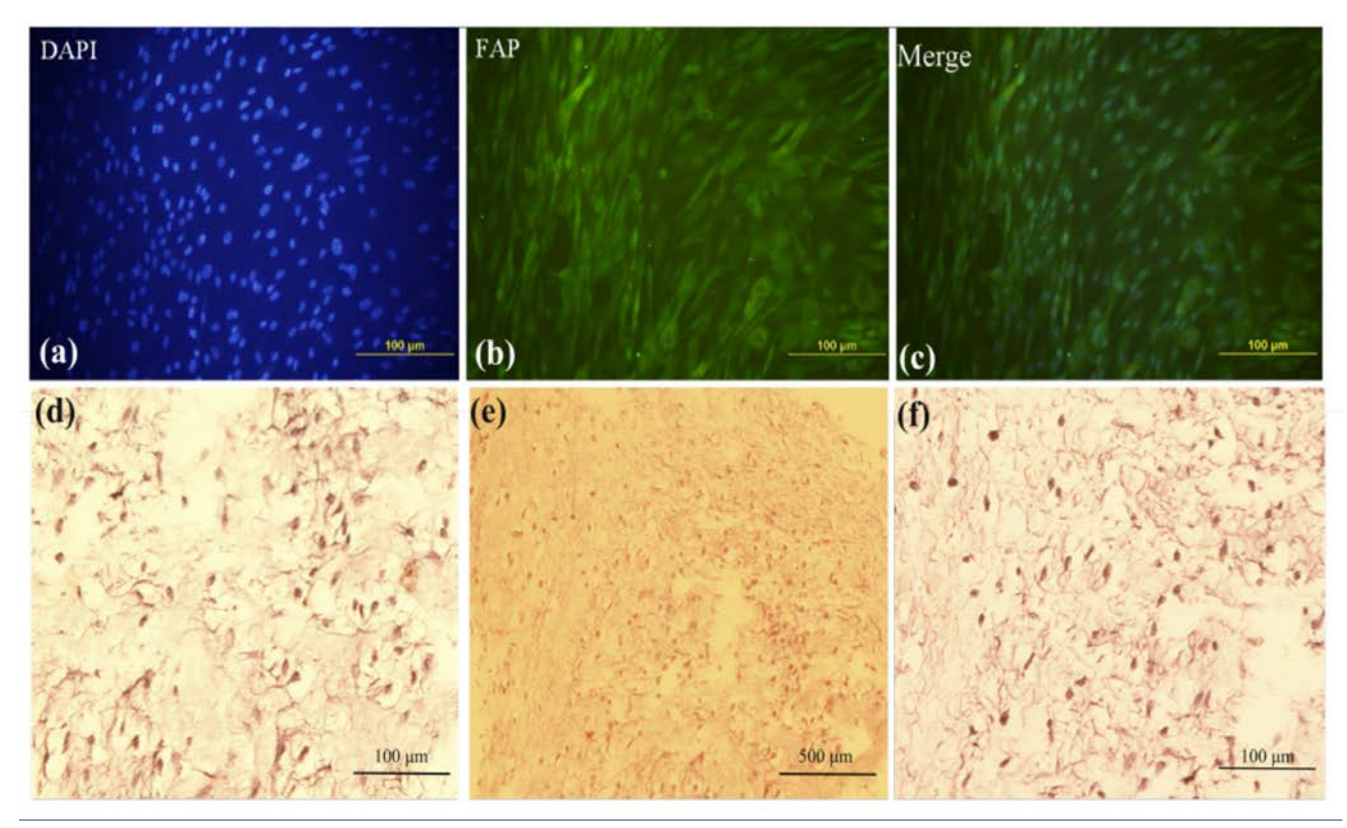


Figure 2. CAF characterization. **a-c**) ICC of stage IV CAFs stained with rabbit anti-FAP and secondary FITC-conjugated goat anti-rabbit IgG. Tumor tissues were sectioned and immunostained with the same primary antibody. The tissues stained positive for FAP-expressing cells; **d**) stage II tumor tissue, 40x magnification; **e**) stage II tumor tissues, 20x magnification; **f**) stage IV tumor tissues, 40x magnification.





CAFs were successfully isolated from both stages II and IV tumors, with characterization revealing similar phenotypes. We further investigated the expression of enzymes involved in inflammation, known to contribute to immune suppression within the TME. We compared the expression of enzymes involved in inflammation between stages II and IV CAFs.²¹ IDO1 is a wound-healing enzyme²² and plays a critical role in immune suppression through

the oxidative degradation of L-tryptophan.²³ It is primarily induced by interferon (IFN)- γ , interleukin (IL)-12, and IL-18.²⁴ Additionally, prostaglandin E2 (PGE2) can upregulate IDO1 expression, although this process requires co-stimulatory signals from other cytokines, such as tumor necrosis factor (TNF)- α .²⁵ IDO1 is expressed not only by cancer cells but also by activated stromal cells, including CAFs. It contributes to T cell exhaustion, in

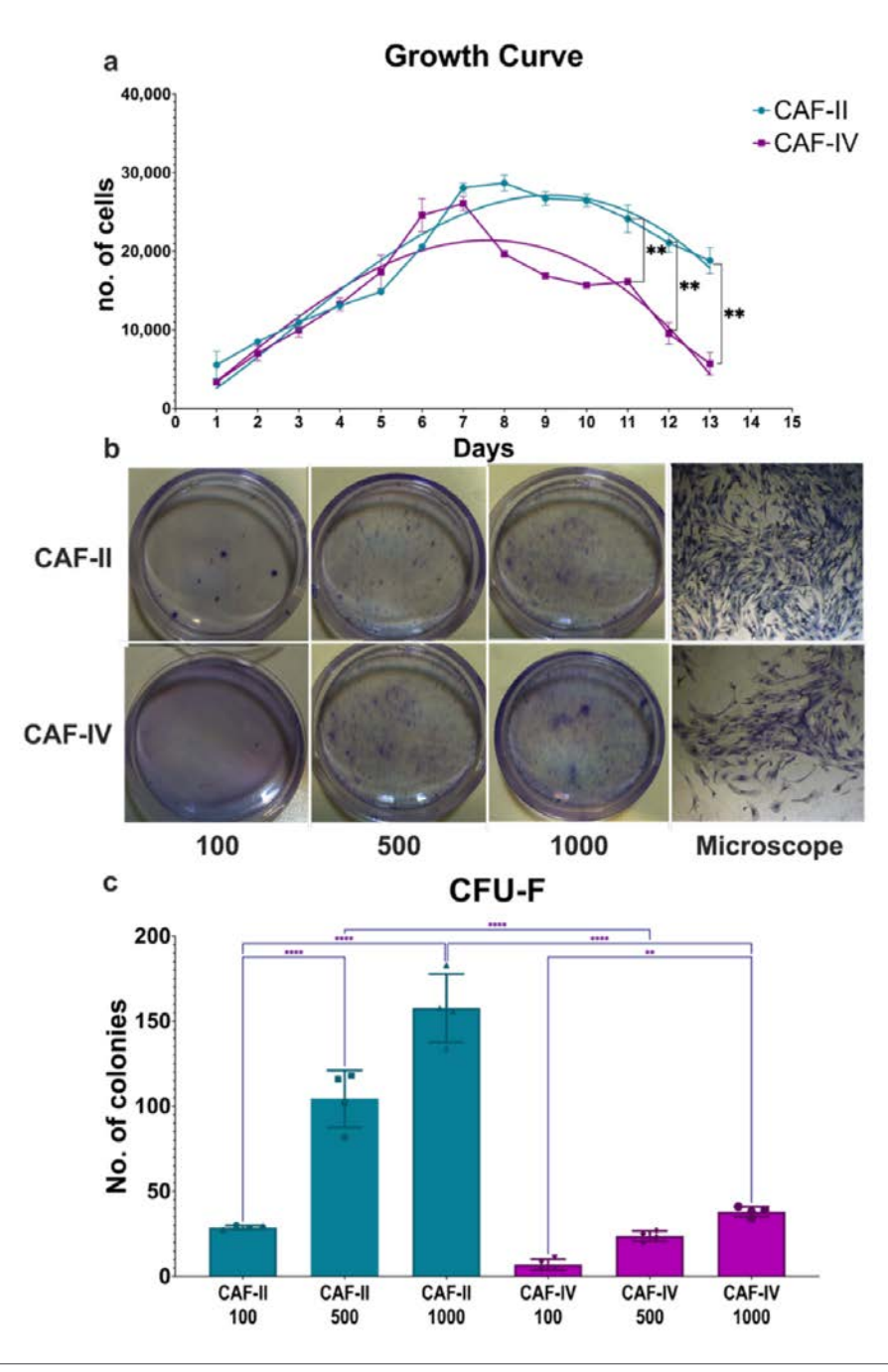


Figure 3. Growth curve and CFU-F assay in isolated CAFs. **a)** Growth curves of isolated CAFs were assessed for their capacities to expand *in vitro*, and demonstrated higher proliferation capacities of CAF-II cells. The difference was evident from day 8 and was statistically significant from day 11 to day 13 (p<0.05). Accordingly, the CFU-F assay of isolated CAFs revealed significantly higher clonogenic potential in CAF-II cells compared to CAF-IV, indicating their greater potential for expansion (p<0.05). 100, 500, and 1,000 cells were seeded in 90 mm dishes, and after 14 days, the media was removed and cells were fixed and stained with crystal violet. **b,c)** The colonies measuring >2 mm in diameter, photographed on dishes, or consisting of >50 cells, as seen in the microscopic view, were counted.



part by promoting PD-L1 expression in dendritic cells.²⁶ Moreover, IDO1 activity is sensitive to nitric oxide (NO),²⁷ which can inhibit its function. Our findings, supported by previous studies, indicate that in more advanced tumor stages, increased expression of iNOS leads to reduced IDO1 expression, suggesting a regulatory interplay between NO signaling and IDO1-mediated immunosuppression.

A cross-regulatory pathway exists between the IDO and NO pathways, with inhibition of one pathway stimulating the other.²⁸ In the mentioned study, it was shown that immune suppression was only abrogated when both pathways were inhibited. The dual role of iNOS in cancer, with both pro- and anti-tumor effects, underscores the complexity of immune modulation in cancer therapy.²⁹

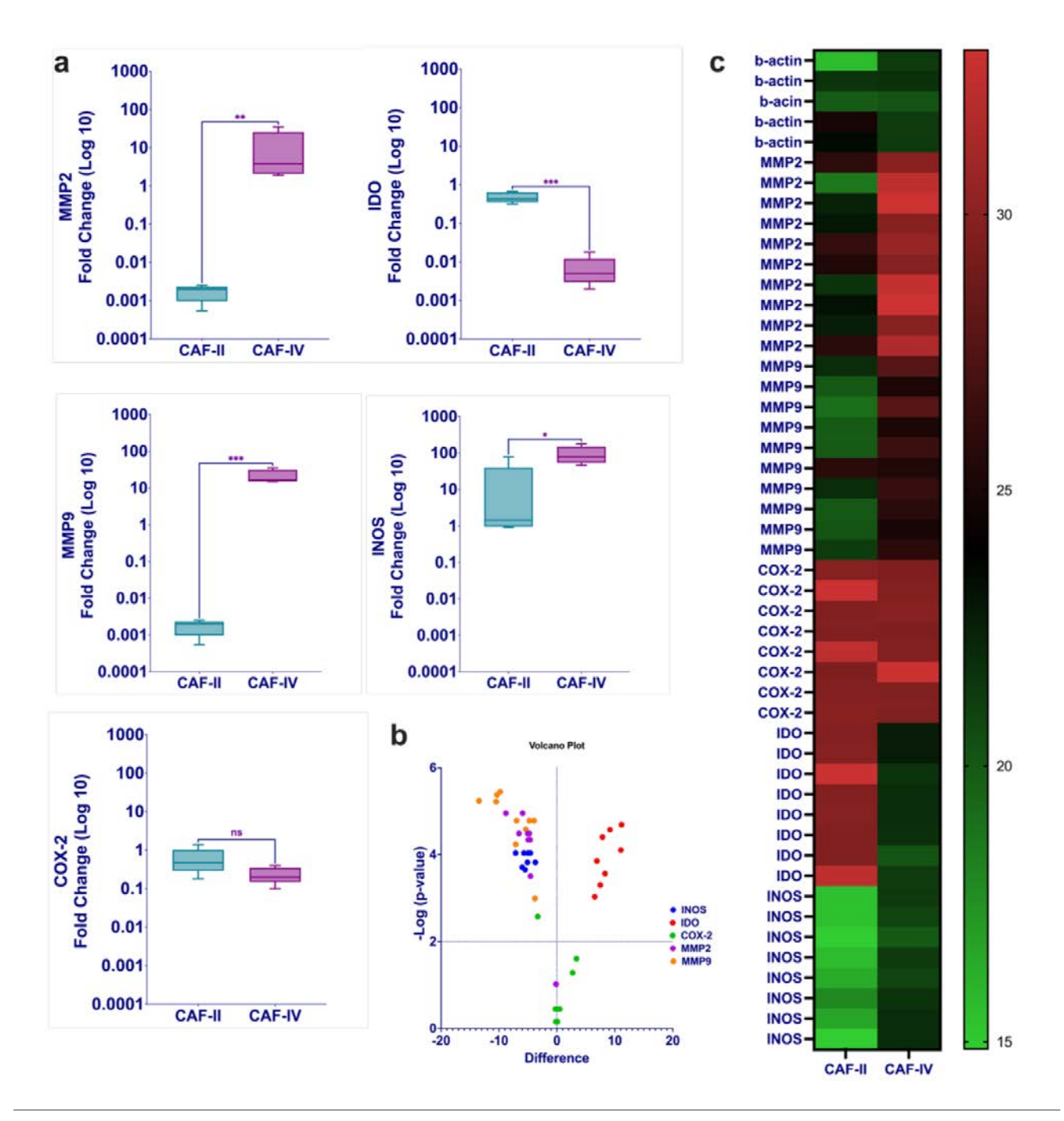


Figure 4. a) Relative gene expression analysis, **b**) volcano plot, and **c**) heatmap comparison of MMP2, MMP9, COX-2, IDO1, and iNOS expression. Total cellular RNAs were extracted from CAFs in passage 2. cDNA was synthesized, and real-time PCR was used to compare gene expressions. CAF-IV was used as the control, and CAF-II as the target in the REST analysis. **a**) A significant increase in IDO1 expression was observed in CAF-II, and iNOS expression was significantly higher in CAF-IV. (***p<.000). COX-2 had similar expression in both stages (p>05), MMP9 was higher in stage II, and MMP2 was higher in stage IV, although not statistically significant.





Conclusions

The functions of CAFs in immune suppression have garnered significant attention, but the identification of different CAF subtypes with distinct functions complicates therapy development. Further research is required to elucidate the distinct functions of individual CAF subtypes and to understand their specific implications for cancer therapy. These studies may help to uncover the diverse roles of each subtype, paving the way for more targeted and effective therapeutic strategies.

References

- Xu Y, Gong M, Wang Y, et al. Global trends and forecasts of breast cancer incidence and deaths. Sci Data 2023;10:334.
- Jonkers J, Derksen PWB. Modeling metastatic breast cancer in mice. J Mammary Gland Biol Neoplasia 2007;12:191-203.
- Lindsay SJ, Rahbari R, Kaplanis J, et al. Similarities and differences in patterns of germline mutation between mice and humans. Nat Commun 2019;10:4053.
- de Jong M, Maina T. Of mice and humans: are they the same?
 Implications in cancer translational research. J Nucl Med 2010;51:501-4.
- Terpstra AHM. Differences between humans and mice in efficacy of the body fat lowering effect of conjugated linoleic acid: role of metabolic rate. J Nutr 2001;131:2067-8.
- Demetrius L. Of mice and men: when it comes to studying ageing and the means to slow it down, mice are not just small humans. EMBO Rep 2005;6:S39-44.
- Hansen K, Khanna C. Spontaneous and genetically engineered animal models; use in preclinical cancer drug development. Eur J Cancer 2004;40:858-80.
- Setlow RB. Human cancer: etiologic agents/dose responses/DNA repair/cellular and animal models. Mutat Res 2001:477:1-6.
- Yang Y, Yang HH, Hu Y, et al. Immunocompetent mouse allograft models for development of therapies to target breast cancer metastasis. Oncotarget 2017;8:30621.
- Ruggeri BA, Camp F, Miknyoczki S. Animal models of disease: pre-clinical animal models of cancer and their applications and utility in drug discovery. Biochem Pharmacol 2014;87:150-61.
- Szadvári I, Krizanova O, Babula P. Athymic nude mice as an experimental model for cancer treatment. Physiol Res 2016;65.
- Olson B, Li Y, Lin Y, et al. Mouse models for cancer immunotherapy research. Cancer Discov 2018;8:1358-65.
- 13. Karamitopoulou E. Tumour microenvironment of pancreatic cancer: immune landscape is dictated by molecular and histopathological features. Br J Cancer 2019;121:5-14.
- Langroudi L, Hasan ZM, Ardeshirylajimi A, Soleimani M. Isolation and characterization of a new cell line from spontaneous mouse mammary tumour, MBL-6, for in vivo cancer

- studies. Vet Sci Dev 2017;7.
- Edelstein-Keshet L. Mathematical models in biology. SIAM; 2005.
- 16. Amin MB, Greene FL, Edge SB, et al. The Eighth Edition AJCC Cancer Staging Manual: Continuing to build a bridge from a population-based to a more "personalized" approach to cancer staging. CA Cancer J Clin 2017;67:93-9.
- Faustino-Rocha A, Oliveira PA, Pinho-Oliveira J, et al. Estimation of rat mammary tumor volume using caliper and ultrasonography measurements. Lab Anim (NY) 2013;42:217-24
- 18. Yang CH, Wang SJ, Lin ATL, et al. Evaluation of prostate volume by transabdominal ultrasonography with modified ellipsoid formula at different stages of benign prostatic hyperplasia. Ultrasound Med Biol 2011;37:331-7.
- Alimohamadi Y, Sepandi M. Sample Size in Animal Studies (The number of laboratory animals in a Research study). Iran J Med Microbiol 2022;16.
- Lavie D, Ben-Shmuel A, Erez N, Scherz-Shouval R. Cancerassociated fibroblasts in the single-cell era. Nat Cancer 2022;3:793-807.
- Lemos H, Huang L, Prendergast GC, Mellor AL. Immune control by amino acid catabolism during tumorigenesis and therapy. Nat Rev Cancer 2019;19:162-75.
- Bandeira LG, Bortolot BS, Cecatto MJ, et al. Exogenous tryptophan promotes cutaneous wound healing of chronically stressed mice through inhibition of TNF-α and IDO activation. PLoS One 2015;10:e0128439.
- 23. Hornyák L, Dobos N, Koncz G, et al. The role of indoleamine-2, 3-dioxygenase in cancer development, diagnostics, and therapy. Front Immunol 2018;9:340144.
- 24. Deng J, Li D, Huang X, et al. Interferon-γ enhances the immunosuppressive ability of canine bone marrow-derived mesenchymal stem cells by activating the TLR3-dependent IDO/kynurenine pathway. Mol Biol Rep 2022;49:8337-47.
- Braun D, Longman RS, Albert ML. A two-step induction of indoleamine 2, 3 dioxygenase (IDO) activity during dendriticcell maturation. Blood 2005;106:2375-81.
- Cheng JT, Deng YN, Yi HM, et al. Hepatic carcinoma-associated fibroblasts induce IDO-producing regulatory dendritic cells through IL-6-mediated STAT3 activation. Oncogenesis 2016;5:e198.
- Biswas P, Stuehr DJ. Indoleamine dioxygenase and tryptophan dioxygenase activities are regulated through control of cell heme allocation by nitric oxide. J Biol Chem 2023;299.
- 28. Ye QX, Xu LH, Shi PJ, et al. Indoleamine 2, 3-dioxygenase and inducible nitric oxide synthase mediate immune tolerance induced by CTLA4Ig and anti-CD154 hematopoietic stem cell transplantation in a sensitized mouse model. Exp Ther Med 2017;14:1884-91.
- Vafaei S, Taheri H, Hajimomeni Y, et al. The role of NLRP3 inflammasome in colorectal cancer: Potential therapeutic target. Clin Transl Oncol 2022;24:1881-9.

